Two-site Bose-Hubbard model with nonlinear tunneling: Classical and quantum analysis

D. Rubeni, J. Links,[*] and P. S. Isaac

School of Mathematics and Physics, The University of Queensland, Brisbane, QLD 4072, Australia

A. Foerster

Instituto de Física da UFRGS, Avenida Bento Gonçalves 9500, Agronomia, Porto Alegre, RS, Brazil
(Received 11 October 2016; published 6 April 2017)

The extended Bose-Hubbard model for a double-well potential with atom-pair tunneling is studied. Starting with a classical analysis we determine the existence of three quantum phases: self-trapping, phase-locking, and Josephson states. From this analysis we build the parameter space of quantum phase transitions between degenerate and nondegenerate ground states driven by the atom-pair tunneling. Considering only the repulsive case, we confirm the phase transition by the measure of the energy gap between the ground state and the first excited state. We study the structure of the solutions of the Bethe ansatz equations for a small number of atoms. An inspection of the roots for the ground state suggests a relationship to the physical properties of the system. By studying the energy gap we find that the profile of the roots of the Bethe ansatz equations is related to a quantum phase transition.

I. INTRODUCTION

The Bose-Hubbard model for a double-well potential has been extensively studied since the experimental realization of Bose-Einstein condensates (BECs). This simple model can well describe Josephson oscillations and nonlinear self-trapping of BECs in a double-well trap [1] with weak atom-atom interactions. Due to its simplicity, this model has been investigated widely by many authors using various methods, such as the Gross-Pitaevskii approximation [2], mean-field theory [3,4], the quantum phase model [5], and the Bethe ansatz method [6], providing insights into many intriguing phenomena. For example, it is well known that this model presents a *quantum phase transition* separating a delocalized from a self-trapped phase [7,8], which has been observed through parity-symmetry breaking [9].

The tunneling dynamics of a few atoms loaded in a double-well trap has been studied by varying the interaction strength from the weak to the strong limit, and the existence of *correlated tunneling* has been confirmed. The study [10] was the first to directly observe atom-pair tunneling processes, in a sample of rubidium atoms in the few-atom limit. This was achieved through the use of superimposed periodic potentials to create an array of double-well potentials. It was shown that the tunneling character changes from Rabi oscillation to an atom-pair cotunneling process with increasing interaction. Complementary theoretical analysis has also been presented in terms of two-body quantum mechanics [11].

It is known that the two-mode Bose-Hubbard model (TMBH) should be modified by a nonlinear tunneling term in the derivation of a two-mode approximation from the many-body nonlinear Schrödinger equation [12,13]. However, this term is most commonly omitted because the nonlinear tunneling coupling is several orders of magnitude smaller than the linear tunneling strength. However, in [14] it was argued that the inclusion of an atom-pair tunneling term

in theoretical calculations produces a noticeably better fit with the experimental data in [10]. Following from this finding, there has been a great deal of effort devoted to the theoretical development of this subject [15–18]. Among these is a proposal to use lattice shaking techniques in order to tune and amplify, the atom-pair tunneling strength [16]. This raises the prospect of investigations into atom-pair tunneling effects beyond the few-atom setup in [10].

In anticipation of further developments in this direction, here we adopt a Hamiltonian including the atom-pair tunneling term to describe BECs in a double-well potential. The extended two-mode Bose-Hubbard model (eTMBH) is described by the Hamiltonian

$$
\begin{aligned}
H = {} & U_1 \hat{n}_1^2 + U_2 \hat{n}_2^2 - \frac{1}{2}\Delta(\hat{n}_1 - \hat{n}_2) - \frac{J}{2}(\hat{a}_1^\dagger \hat{a}_2 + \hat{a}_2^\dagger \hat{a}_1) \\
& - \frac{\Omega}{2}(\hat{a}_1^\dagger \hat{a}_1^\dagger \hat{a}_2 \hat{a}_2 + \hat{a}_2^\dagger \hat{a}_2^\dagger \hat{a}_1 \hat{a}_1),
\end{aligned} \tag{1}
$$

where $\{\hat{a}_j, \hat{a}_j^\dagger \,|\, j = 1, 2\}$ are the creation and annihilation operators for well j, associated, respectively, with two bosonic Heisenberg algebras and satisfying the following commutation relations:

$$
[\hat{a}_i, \hat{a}_j^\dagger] = \delta_{ij}, [\hat{a}_i, \hat{a}_j] = [\hat{a}_i^\dagger, \hat{a}_j^\dagger] = 0.
$$

Also, $\hat{n}_j = \hat{a}_j^\dagger \hat{a}_j$ is the corresponding boson number operator for each well. Since the Hamiltonian commutes with the total boson number operator $\hat{n} = \hat{n}_1 + \hat{n}_2$, the total number of bosons n is conserved and it is convenient to restrict ourselves to a subspace of constant n. The coupling U_j provides the strength of the scattering interaction between bosons in the well j and may be attractive ($U_j < 0$) or repulsive ($U_j > 0$). The parameter Δ is the external potential, which corresponds to an asymmetry between the condensates, J is the coupling for the tunneling, and Ω is the coupling for the atom-pair tunneling process. The change $J \rightarrow -J$ corresponds to the unitary transformations $\hat{a}_1 \rightarrow \hat{a}_1$, $\hat{a}_2 \rightarrow -\hat{a}_2$, while $\Delta \rightarrow -\Delta$ corresponds to $\hat{a}_1 \leftrightarrow \hat{a}_2$. Therefore we restrict our analysis to the case of $J, \Delta \geqslant 0$.

———————
[*]jrl@maths.uq.edu.au

Undertaking a classical analysis we obtain the fixed points of the system in the large-n limit and find three distinct phases for the ground state. Under the right conditions the system may undergo a quantum phase transition. The results in some particular cases allow us to identify a parameter space of quantum phase transitions. We then confirm that this parameter space is associated with quantum phase tranitions of the system through studies of the energy gap.

Motivated by the results in [9–11], and also by the discussion in [14] of the case of a low particle number, we then present the exact solution for this model using the Bethe ansatz approach. By this method one can have access to the ground state through the solution of a set of Bethe ansatz equations (BAEs). A careful observation of the behavior of solutions of these equations for the ground state, as we vary some parameters of the Hamiltonian, suggests a connection between the behavior of roots of the BAEs and the physical behavior of this model. This is exactly what we expect to happen in quantum phase transitions.

This paper is organized as follows: in Sec. II we analyze the eTMBH model through bifurcations in a classical analysis. These are used to indicate potential quantum phase transitions. We find the fixed points for the special case $\Delta = 0$, $U_1 = U_2$ and build a parameter space of phase transitions. A comparison is made between the classical predictions and the energy gap. In Sec. III we present the Bethe ansatz solution and investigate the distribution of the roots of the Bethe ansatz equations for the ground state. In Sec. IV we summarize our results.

II. CLASSICAL ANALYSIS

We start our analysis with a semiclassical treatment. We study the phase space of this system, in particular, determining the fixed points. It is found that for certain coupling parameters bifurcations of the fixed points occur, and we can determine a parameter-space diagram which classifies the fixed points.

For this second-quantized model, if the particle number n is large enough, the system can be well described in the classical approximation [19], where creation or annihilation operators can be replaced by complex numbers (n_j, θ_j) such as

$$\hat{a}_j \to e^{i\theta_j}\sqrt{n_j}, \quad \hat{a}_j^\dagger \to \sqrt{n_j} e^{-i\theta_j}.$$

By introducing the canonically conjugate variables *population imbalance* z and *phase difference* θ, defined by

$$z = \frac{1}{n}(n_1 - n_2), \quad \theta = \frac{n}{2}(\theta_1 - \theta_2),$$

the system can be described by the classical Hamiltonian

$$\mathcal{H} = \frac{nJ}{4}(\lambda(1 + z^2) - \gamma(1 - z^2)\cos(4\theta/n)$$
$$- 2\sqrt{1 - z^2}\cos(2\theta/n) - 2\beta z), \quad (2)$$

where

$$\lambda = \frac{n}{J}(U_1 + U_2), \quad \beta = \frac{n}{J}\left(\frac{\Delta}{n} - U_1 + U_2\right), \quad \text{and} \quad \gamma = \frac{n\Omega}{J}$$
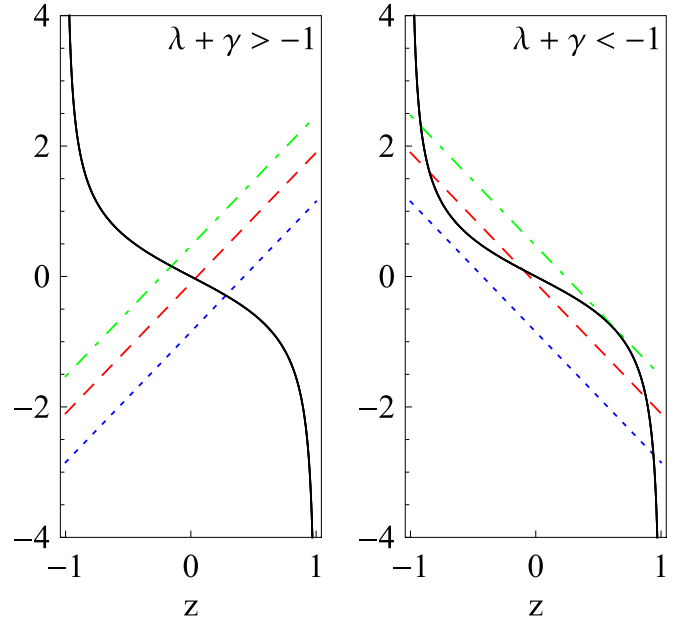

FIG. 1. Graphical solution of Eq. (5). The crossing between the straight line [left-hand side of Eq. (5)] and the curve [right-hand side of Eq. (5)] for different values of $\lambda + \gamma$ and β represents the solution(s) for each case. There is just one solution on the left ($\lambda + \gamma \geqslant -1$), while there are either one, two, or three solutions on the right ($\lambda + \gamma < -1$).

are the coupling parameters. Hamilton's equations of motion are given by

$$\dot{z} = -J\sin(2\theta/n)(2\gamma\cos(2\theta/n) - 2\gamma z^2\cos(2\theta/n)$$
$$+ \sqrt{1 - z^2}), \quad (3)$$

$$\dot{\theta} = \frac{nJ}{2}\left(-\beta + \gamma z\cos(4\theta/n) + \frac{z\cos(2\theta/n)}{\sqrt{1 - z^2}} + \lambda z\right). \quad (4)$$

In the limit $\gamma \to 0$ we recover the equations of motion of the TMBH [20]. The fixed points can be readily derived from the condition $\dot{z} = \dot{\theta} = 0$. Due to periodicity of the solutions, below we restrict ourselves to $2\theta/n \in [-\pi, +\pi]$. This leads to the following classification.

(i) $\theta = 0$ and z is a solution of

$$-\beta + z(\gamma + \lambda) = -\frac{z}{\sqrt{1 - z^2}}, \quad (5)$$

which has one solution for $\lambda + \gamma \geqslant -1$, while it may have one, two, or three solutions for $\lambda + \gamma < -1$. In Fig. 1 we present a graphical solution of (5).

(ii) $2\theta/n = \pm\pi$ and z is a solution of

$$-\beta + z(\gamma + \lambda) = \frac{z}{\sqrt{1 - z^2}}. \quad (6)$$

This equation has one solution for $\lambda + \gamma \leqslant 1$ and has either one, two, or three real solutions for $\lambda + \gamma > 1$.

(iii) $z = \beta/(\lambda - \gamma)$ and θ is a solution of

$$\cos(2\theta/n) = \frac{-1}{2\gamma\sqrt{1 - \left(\frac{\beta}{\lambda - \gamma}\right)^2}}, \quad (7)$$

which has two real solutions for $\gamma \notin [-1/2, 1/2]$ and $|\lambda - \gamma| \geqslant 2|\beta\gamma|(4\gamma^2 - 1)^{-1/2}$.

From Eqs. (5) and (6) we can determine that there are fixed point bifurcations for certain choices of the coupling parameters. These bifurcations allow us to divide the coupling-parameter space into three regions. A standard analysis shows that the boundary between the regions obeys the relation

$$\lambda + \gamma = \pm(1 + |\beta|^{\frac{2}{3}})^{\frac{3}{2}} \qquad (8)$$

(see [21] for details). Equation (8) leads to a partition of the parameter space into three regions, depicted in Fig. 2(a). In the absence of the external potential, i.e., $\beta = 0$, we have a fixed point bifurcation given by $\lambda = \pm 1 - \gamma$. See Fig. 2(b). Irrespective of the nature of the bifurcation, it has been observed in classical analyses [22,23] that fixed points can be used to identify quantum phase transitions. This model therefore becomes a promising candidate to study.

The conditions for the existence of solutions to Eq. (7) allow us to build a parameter-space diagram as depicted in Fig. 2(c). The boundary between regions satisfies the relation

$$\lambda - \gamma = \pm 2|\beta\gamma|(4\gamma^2 - 1)^{-1/2}. \qquad (9)$$

A. Fixed points and eigenstates for $\beta = 0$

In the following we study the solutions of the fixed point equations (5)–(7) with $\beta = 0$ by the consideration of two main reasons: (i) nonzero values of Δ do not significantly alter the behavior of the system, just shift the energy levels [7]; and (ii) many of the experimental realizations with these systems are made on the condition of zero external potential and equal interaction between atoms in each well [10]. In Fig. 2(b) we see the parameter-space diagram for Eqs. (5) and (6) with $\beta = 0$, while Fig. 2(d) shows the parameter-space diagram for Eq. (7) for $\beta = 0$.

It has been demonstrated that the fixed points of phase-space level curves are the points of extreme energy corresponding to eigenstates of the system [24]. Since the fixed point bifurcations change the topology of the level curves, qualitative differences can be observed between each of the three regions. For further analysis, it is useful to assign to each fixed point (θ_{FP}, z_{FP}) a point P_j in the phase space as follows:

$$P_1 \rightarrow (0, 0),$$
$$P_2 \rightarrow (0, \pm\sqrt{1 - 1/(\lambda + \gamma)^2}),$$
$$P_3 \rightarrow (\pm\text{arcsec}(-2\gamma), 0),$$
$$P_4 \rightarrow (\pm\pi, 0),$$
$$P_5 \rightarrow (\pm\pi, \pm\sqrt{1 - 1/(\lambda + \gamma)^2}).$$

Figure 3 shows the typical character of the level curves in region I. There are three fixed points for $\theta = 0$ and one fixed point for $2\theta/n = \pm\pi$. When $\gamma < \lambda$ the ground state is associated with the fixed points P_3. These two states are called *phase-locking states*, with zero population imbalance and tunable relative phase unequal to 0 or π [see Fig. 3(a)]. This phase-locking state was also identified in [14]. The highest energetic states correspond to the fixed points P_4. At $\gamma = \lambda$ the system changes to a special state: the ground state is over a "ring" instead a of point, as depicted in
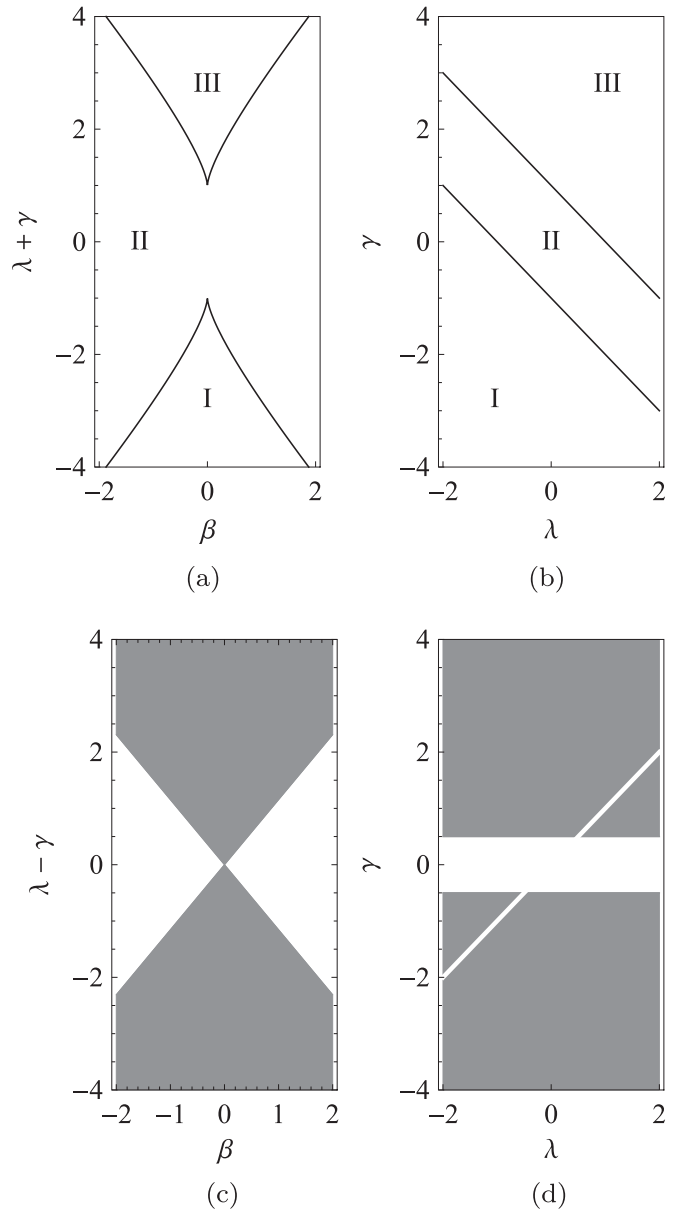

FIG. 2. Coupling parameter-space diagrams characterizing the solutions for the fixed points $\dot{z} = \dot{\theta} = 0$. (a) Parameter space for Eqs. (5) and (6) with $\beta \neq 0$. The boundaries between the regions are given by Eqs. (8). At the boundary between region I and region II there are two solutions for $\theta = 0$ and one solution for $2\theta/n = \pm\pi$, while there is one solution for $\theta = 0$ and two solutions for $2\theta/n = \pm\pi$ at the boundary between region II and region III. (b) Parameter space for Eqs. (5) and (6) with $\beta = 0$. The boundaries between the regions obey the equations $\gamma = \pm 1 - \lambda$. In both cases, there are three solutions for $\theta = 0$ and one solution $2\theta/n = \pm\pi$ in region I; in region II, we have one solution for $\theta = 0$ and one solution for $2\theta/n = \pm\pi$; and in region III, there is one solution for $\theta = 0$ and three solutions for $2\theta/n = \pm\pi$. (c) Example of parameter space for Eq. (7) with $\beta \neq 0$. This equation has only one solution for the values of parameters that lie within the shaded area, with boundaries given by (9), and $|\gamma| > 1/2$. (d) Parameter space for Eq. (7) with $\beta = 0$. This equation has a solution only for the values of parameters that lie within the gray area, with $|\gamma| > \frac{1}{2}$ and $\gamma \neq \lambda$.

Fig. 3(b). This is a transition state, since any small changes in the values of λ and γ alter its nature. When $\gamma > \lambda$ there is an
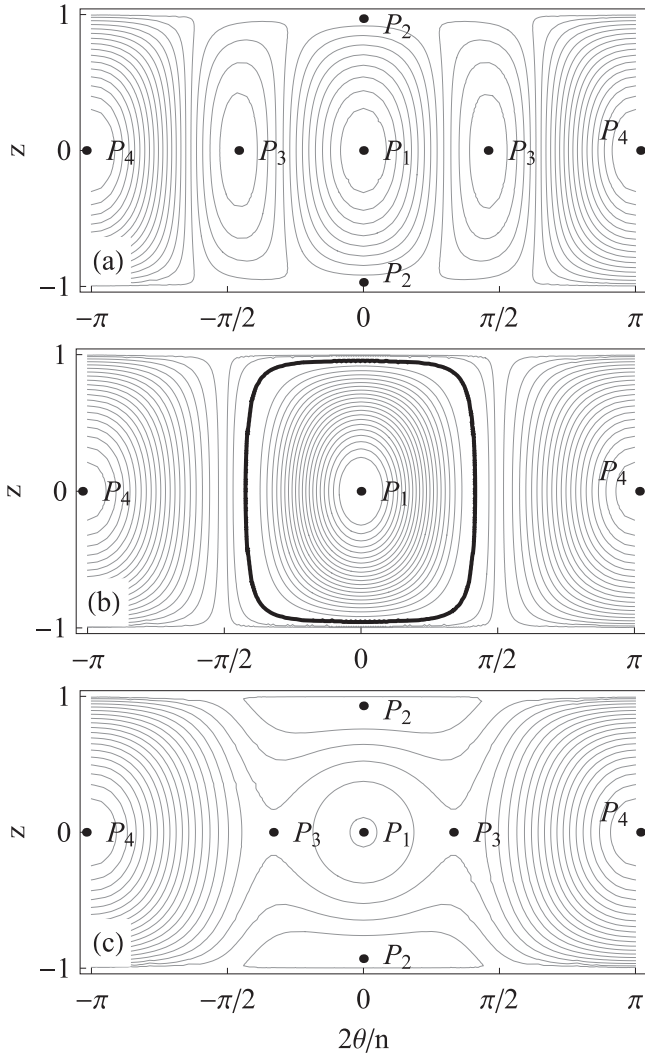
FIG. 3. Level curves of the classical Hamiltonian in region I. The points $\{P_1, \ldots, P_4\}$ denote the fixed points of the Hamiltonian. (a) Parameter values are $n = 100$, $\lambda = -2$, $J = 1$, and $\gamma = -4$. There is a local maximum at P_1 and saddle points at P_2. Global minima are at P_3, while P_4 are global maxima. (b) Parameter values are $n = 100$, $\lambda = -2$, $J = 1$, and $\gamma = -2$. A "ring" emerges as the global minimum. The local and global maxima still occur at P_1 and P_4, respectively. (c) Now the parameter values are $n = 100$, $\lambda = -2$, $J = 1$, and $\gamma = -1$. Global minima are at P_2. There are saddle points at P_3, a local maximum point at P_1, and global maxima at P_4.

abrupt change in the ground state: the minimum energy levels move towards the fixed points P_2. We denote those eigenstates whose corresponding fixed points have a nonzero population imbalance, $z \neq 0$, *self-trapping states*, as depicted in Fig. 3(c). Therefore, now the ground state is a degenerate self-trapping state. This means that at $\gamma = \lambda$ the system undergoes a quantum phase transition from degenerate phase-locking states to degenerate self-trapping states. Further changes in the coupling parameters modify the fixed point configuration but no longer alter the nature of the ground state. Table I provides a detailed classification of all the fixed points in region I as the parameters λ and γ change.

TABLE I. Configuration of fixed points and associated states in region I. GS, ground state; HES, highest excited state; lmax, local maximum; sp, saddle point.

Region I	P_1	P_2	P_3	P_4	P_5
$\gamma < \lambda$	lmax	sp	GS	HES	–
$-1/2 > \gamma > \lambda$	lmax	GS	sp	HES	–
$-1/2 < \gamma < 1/2$	sp	GS	–	HES	–
$\gamma > 1/2$	sp	GS	HES	sp	–

Figure 4(a) illustrates the configuration of the fixed points when the coupling parameters are tuned to cross over from region I into region II. There is one fixed point for $\theta = 0$ and one for $2\theta/n = \pm\pi$. If $\gamma > -1/2$, the fixed point P_1 becomes associated with the ground state, with zero population imbalance and zero relative phase, with the presence of tunneling of atoms between the wells because of the weak interaction. We call this state a *Josephson state*. Therefore, when crossing the boundary $\gamma = -1 - \lambda$, the system undergoes a quantum phase transition to a nondegenerate Josephson state. Highest excited states are related to the global maxima at P_3. If $\gamma < -1/2$, there is another quantum phase transition: the global minimum, related to degenerate phase-locking states, emerges at P_3 [see Fig. 4(b)]. Highest energy states are associated with the fixed point P_4 for any $\lambda < 1/2$. Table II summarizes how the fixed point configurations change along with λ and γ.
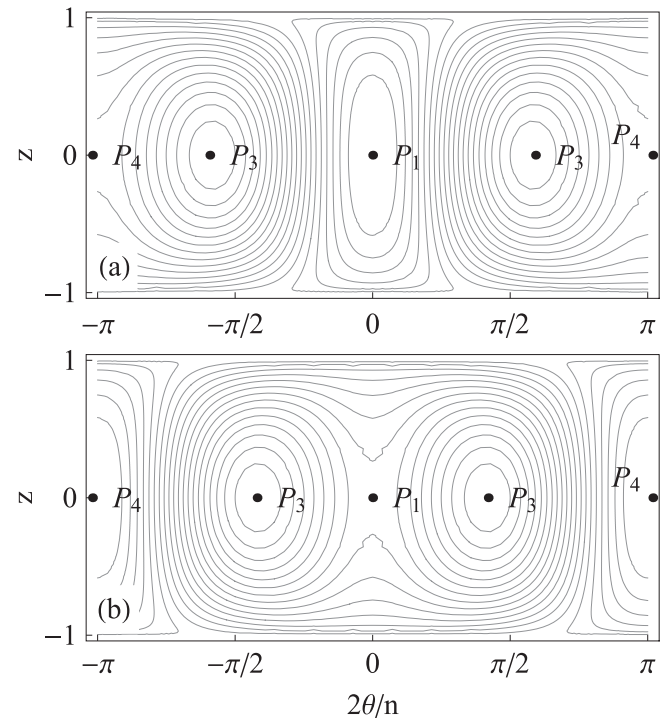

FIG. 4. Typical level curves of the classical Hamiltonian in region II. The points $\{P_1, \ldots, P_4\}$ denote the fixed points of the Hamiltonian. (a) Parameter values are $n = 100$, $\lambda = -2$, $J = 1$, and $\gamma = 2$. There is a global minimum at P_1, the global maximum is at P_3, and P_4 are saddle points. (b) Parameter values are $n = 100$, $\lambda = 2$, $J = 1$, and $\gamma = -2$. Now the fixed point P_1 turns into a saddle point, while there are global minima at P_3 and global maxima emerge at P_4.

TABLE II. Configuration of fixed points and associated states in region II. GS, ground state; HES, highest excited state; sp, saddle point.

Region II	P_1	P_2	P_3	P_4	P_5
$-1/2 > \gamma$	sp	–	GS	HES	–
$-1/2 < \gamma < 1/2$	GS	–	–	HES	–
$\gamma > 1/2$	GS	–	HES	sp	–

TABLE III. Configuration of fixed points and associated states in region III. GS, ground state; HES, highest excited state; lmin, local minimum; sp, saddle point.

Region III	P_1	P_2	P_3	P_4	P_5
$-1/2 > \gamma$	sp	–	GS	sp	HES
$-1/2 < \gamma < 1/2$	GS	–	–	sp	HES
$1/2 < \gamma < \lambda$	GS	–	sp	lmin	HES
$\gamma > \lambda$	GS	–	HES	lmin	sp

On crossing the parameter-space boundary to region III, the fixed point configuration changes again: there is one fixed point for $\theta = 0$ and three fixed points for $2\theta/n = \pm\pi$. The ground state of the system may be associated with P_3 as a degenerate phase-locking state if $\gamma < -1/2$. New fixed points emerge at P_5 as highest energetic states. If $\gamma > -1/2$, the global minimum changes to P_1 and becomes associated with a nondegenerate Josephson state. Therefore the line $\gamma = -1/2$ defines the boundary for a quantum phase transition [see Figs. 5(a) and 5(b)].

The above discussion gives a general qualitative description of the behavior of the classical system in terms of the three regions identified in the parameter space. Properties of eigenstates as highlighted in Tables I—III enable us to depict the quantum phase transition diagram shown in Fig. 6.
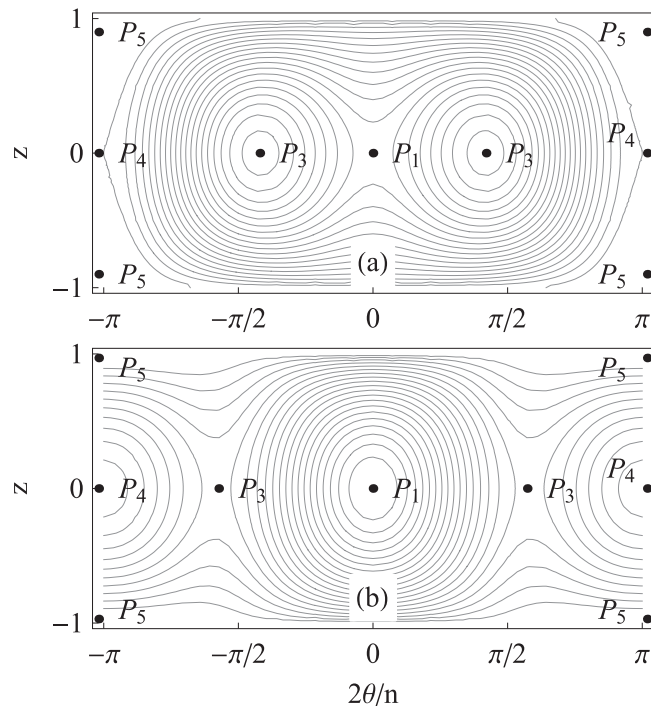
The parameter space (λ, γ) is divided into three regions: the self-trapping, Josephson, and phase-locking phases.

In the next section we restrict ourselves to study of the case $\lambda > 0$ and check the presence of a phase transition as predicted by the phase transition diagram of the behavior of the energy gap.

B. Energy gap

Consider the dimensionless energy gap between the first excited state (FES) and the ground state (GS),

$$\Delta E = \frac{1}{J}(E_{\text{FES}} - E_{\text{GS}}). \tag{10}$$

The values of the parameters for which ΔE goes to 0 identify the location of a quantum phase transition [25]. Using numerical diagonalization of the Hamiltonian, (1), in Fig. 7(a) we plot ΔE as a function of the coupling γ, for $\lambda > 0$ and different values of n. We observe that as n

FIG. 5. Typical level curves of the classical Hamiltonian in region III. The points $\{P_1, \ldots, P_5\}$ denote the fixed points of the Hamiltonian. (a) Parameter values are $n = 100$, $\lambda = 4$, $J = 1$, and $\gamma = -2$. In this scenario P_1 is a saddle point and the global minima are at P_3. The highest energy levels appear at P_5. (b) Parameter values are $n = 100$, $\lambda = 4$, $J = 1$, and $\gamma = 2$. Now the global minima move towards P_1, while P_3 become saddle points. The fixed points P_4 are local minima and the global maxima are still at P_5.
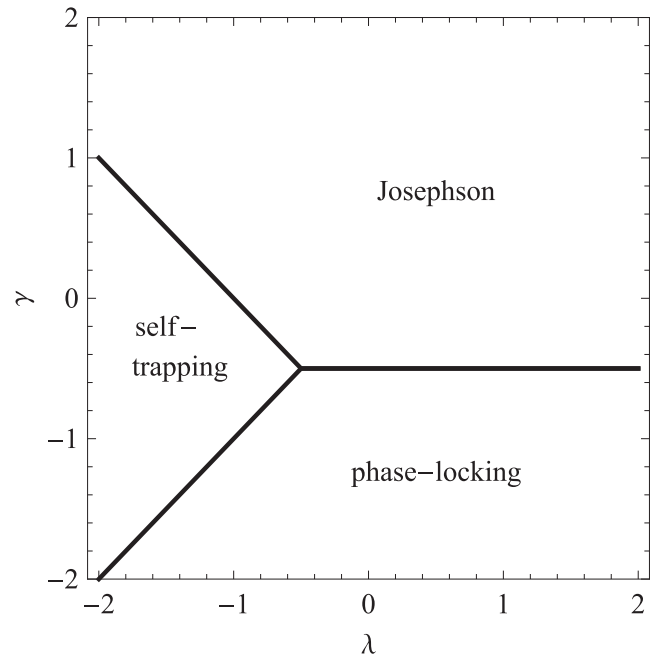

FIG. 6. Parameter space for quantum phase transitions. The boundary between Josephson and phase-locking states is given by $\gamma = -1/2$. The system undergoes a quantum phase transition from phase-locking states to self-trapping states upon crossing the boundary $\gamma = \lambda$, while the limit between the Josephson phase and the self-trapping phase is determined by the line $\gamma = -1 - \lambda$. The threshold coupling occurs at $(\gamma, \lambda) = (-1/2, -1/2)$.
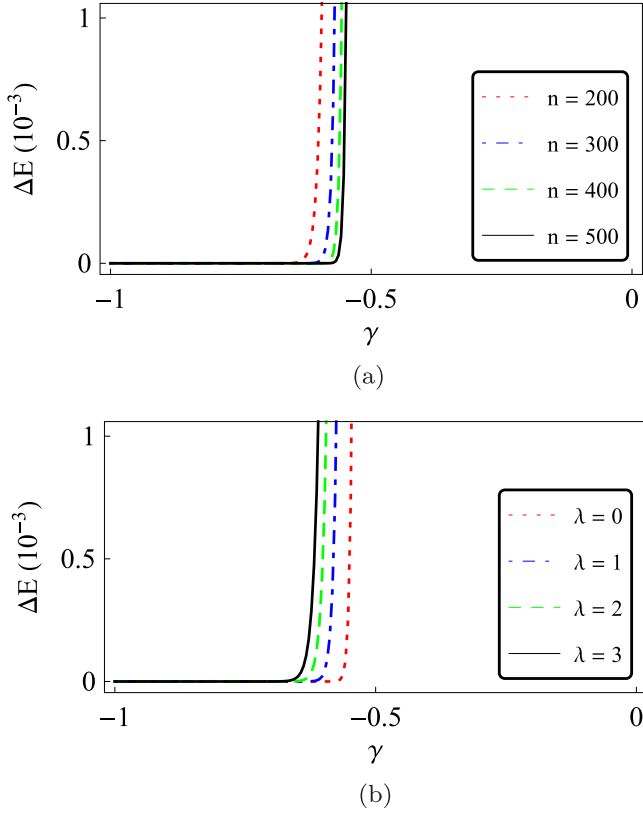
(a)

(b)

FIG. 7. Dimensionless energy gap ΔE as a function of $\gamma = n\Omega/J$ (a) for different values of n and $\lambda = 2$ and (b) for different values of λ and $n = 100$. Values of the parameters are $J = 1$ and $\beta = 0$. These results indicate that the points at which the gap closes lie approximately on the line $\gamma = -1/2$.

increases the dimensionless energy gap decreases and the coupling approaches the point $\gamma = -1/2$. Figure 7(b) shows similar results for fixed n and varying λ. We observe that the occurrence of the vanishing of ΔE, determining the quantum phase transition, fits well with the predicted boundary separating Josephson and phase-locking regions given by $\gamma = -1/2$.

III. BETHE ANSATZ SOLUTION

We now look at obtaining the exact solution of the eTMBH model to investigate low numbers of particles. Diagrams of the Bethe root configurations are provided in Figs. 8 and 9 for the cases $n = 4, 6, 8, 10,$ and 12. In Fig. 10 we also present the energy gap for these low values of n. To obtain the exact solution of the eTMBH model, we follow the work of Enol'skii, Kuznetsov, and Salerno [26]. Starting with the Jordan-Schwinger realization of the su(2) algebra,

$$\hat{S}^+ \to \hat{a}_1^\dagger \hat{a}_2, \quad \hat{S}^- \to \hat{a}_2^\dagger \hat{a}_1, \quad \hat{S}^z \to \frac{\hat{n}_1 - \hat{n}_2}{2},$$

we may write Hamiltonian (1) as

$$H = \frac{k}{8}\hat{n}^2 + \frac{k}{2}(\hat{S}^z)^2 + \alpha\hat{S}^z - \frac{1}{2}J(\hat{S}^+ + \hat{S}^-)$$
$$- \frac{1}{2}\Omega[(\hat{S}^+)^2 + (\hat{S}^-)^2], \tag{11}$$
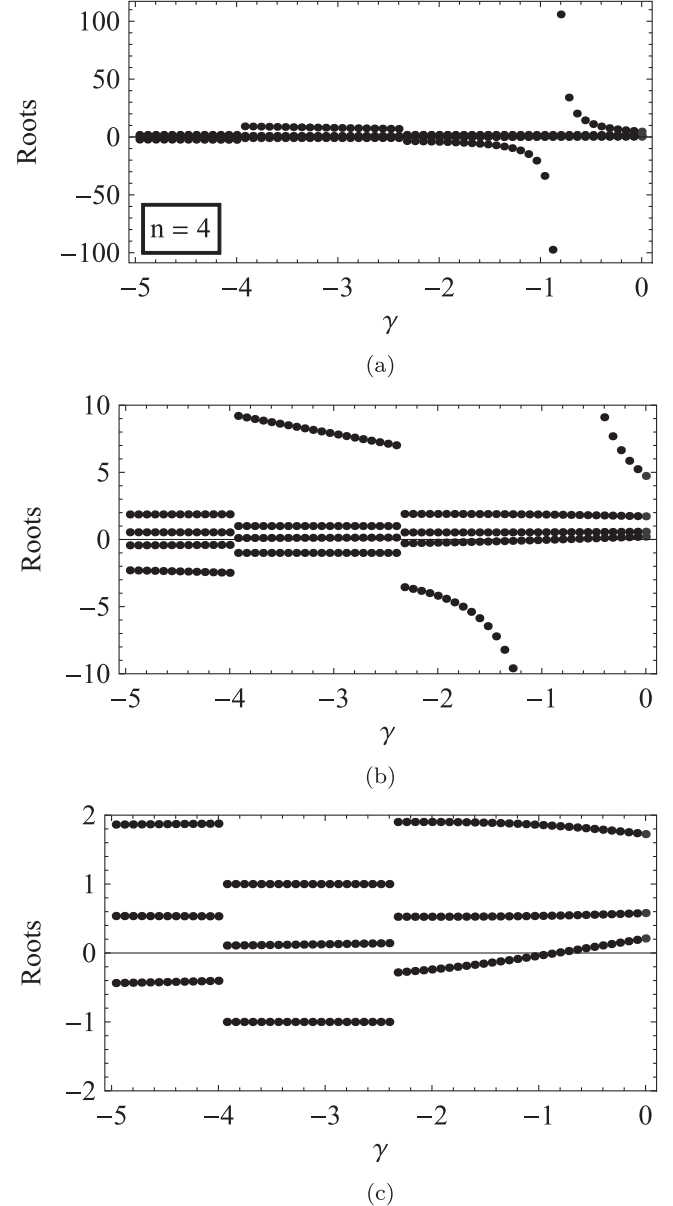

(a)

(b)

(c)

FIG. 8. Solutions of the Bethe ansatz equations (BAE), (15), for the ground state considering the particular case $n = 4$, $k = 1$ and $J = 1$ and different values of γ. In (a)–(c) we look at the same set of solutions at different scales. An abrupt change in the root distribution occurs at $\gamma \simeq -2.38$ and $\gamma \simeq -4.01$.

with $\hat{n} = \hat{n}_1 + \hat{n}_2$, $k = 2(U_1 + U_2)$, and $\alpha = (U_1 - U_2)n - \Delta$. Note that

$$\lambda = \frac{kn}{2J}, \quad \beta = -\frac{\alpha}{J}. \tag{12}$$

If we consider the differential realization of su(2) operators,

$$\hat{S}^+ \to u^2\frac{d}{du} - nu, \quad \hat{S}^- \to -\frac{d}{du}, \quad \hat{S}^z \to u\frac{d}{du} - \frac{n}{2},$$

the Hamiltonian, (11), can be written as

$$H = A(u)\frac{d^2}{du^2} + B(u)\frac{d}{du} + C(u), \tag{13}$$

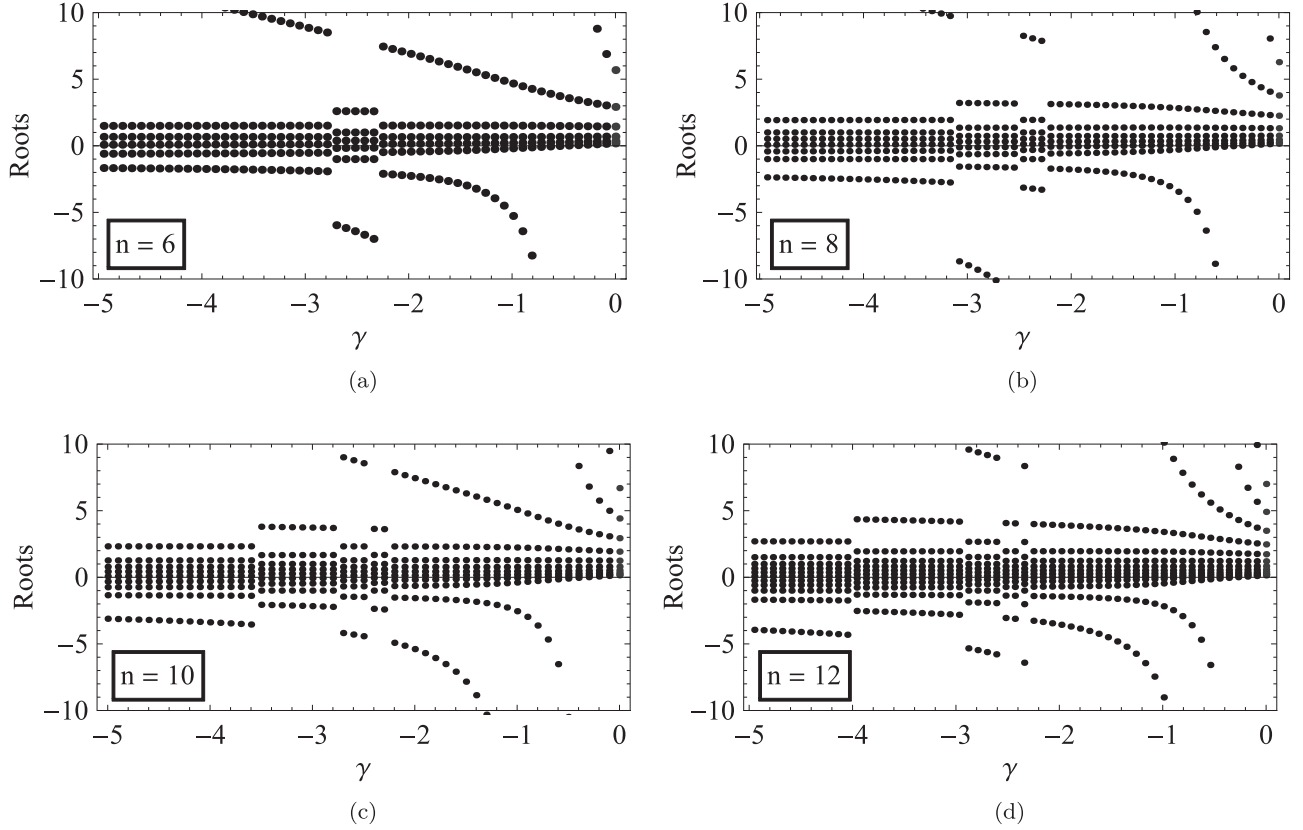FIG. 9. Solutions of the BAE, (15), for the ground state for $n = 6$, 8, 10, and 12, respectively. We set the parameters k and α to satisfy the conditions $\lambda = 2$ and $\beta = 0$ in each case. There are abrupt changes in the distribution of roots for all values of n. The changes occur at (a) $\gamma \simeq -2.30$ and $\gamma \simeq -2.75$; (b) $\gamma \simeq -2.25$, $\gamma \simeq -2.54$, and $\gamma \simeq -3.12$; (c) $\gamma \simeq -2.25$, $\gamma \simeq -2.45$, $\gamma \simeq -2.75$, and $\gamma \simeq -3.54$; and (d) $\gamma \simeq -2.25$, $\gamma \simeq -2.35$, $\gamma \simeq -2.54$, $\gamma \simeq -2.92$, and $\gamma \simeq -3.98$.

with

$$A(u) = \frac{k}{2}u^2 - \frac{\Omega}{2}(u^4 + 1),$$

$$B(u) = \frac{1}{2}\{J(1 - u^2) + [k(1 - n) + 2\alpha]u$$
$$- 2\Omega(1 - n)u^3\},$$

$$C(u) = \frac{k}{4}n^2 - \frac{\alpha}{2}n + \frac{J}{2}nu - \frac{\Omega}{2}n(n - 1)u^2.$$

Solving for the spectrum of the Hamiltonian is then equivalent to solving the eigenvalue equation

$$HQ(u) = EQ(u), \tag{14}$$

where H is represented by (13) and $Q(u)$ is a polynomial function of u of order n. Next, we express $Q(u)$ in terms of its roots υ_j:

$$Q(u) = \prod_{j=1}^{n}(u - \upsilon_j).$$

Evaluating (14) at $u = \upsilon_l$ for each l leads to the set of BAE

$$\frac{-J(\upsilon_l^2 - 1) + [k(1 - n) + 2\alpha]\upsilon_l - 2\Omega(1 - n)\upsilon_l^3}{k\upsilon_l^2 - \Omega(\upsilon_l^4 + 1)}$$
$$= \sum_{j \neq l}^{n} \frac{2}{\upsilon_j - \upsilon_l}, \quad l = 1, \ldots, n. \tag{15}$$

Writing the asymptotic expansion

$$Q(u) \sim u^n - u^{n-1}\sum_{j=1}^{N}\upsilon_j + u^{n-2}\sum_{j=1}^{n-1}\sum_{l=j+1}^{n}\upsilon_j\upsilon_l$$

and considering the terms of order n in (14), the energy eigenvalues are found to be

$$E = \frac{kn^2}{4} + \frac{\alpha n}{2} - \frac{J}{2}\sum_{j=1}^{n}\upsilon_j - \Omega\sum_{j=1}^{n-1}\sum_{l=j+1}^{n}\upsilon_j\upsilon_l. \tag{16}$$

Each set of roots $\{\upsilon_j, j = 1, \ldots, n\}$ of the BAE leads to the energy of the Hamiltonian through (16). Note that the change $J \to -J$ is equivalent to the change $\upsilon_j \to \upsilon_j^{-1}$. For $\alpha = 0$ this shows that each solution set $\{\upsilon_1, \ldots, \upsilon_n\}$ is invariant under $\upsilon_j \to \upsilon_j^{-1}$. In principle, an analytic solution of these equations is not possible. Below, we implement numerical techniques to obtain solutions.

We restrict ourselves to study of the case $k > 0$, $\alpha = 0$ [due to relations (12) this is equivalent to $\lambda > 0$, $\beta = 0$] to investigate the behavior of the BAE solutions around the quantum phase transition line $\gamma = -1/2$. We start by solving the BAE with $\Omega = 0$ for the ground state. In this case, all the roots must be real and positive [27]. If we decrease the value of Ω, the numerical solution of Eq. (15) shows that the ground state always has real roots, but eventually some roots have a smooth transition from positive to negative values. As
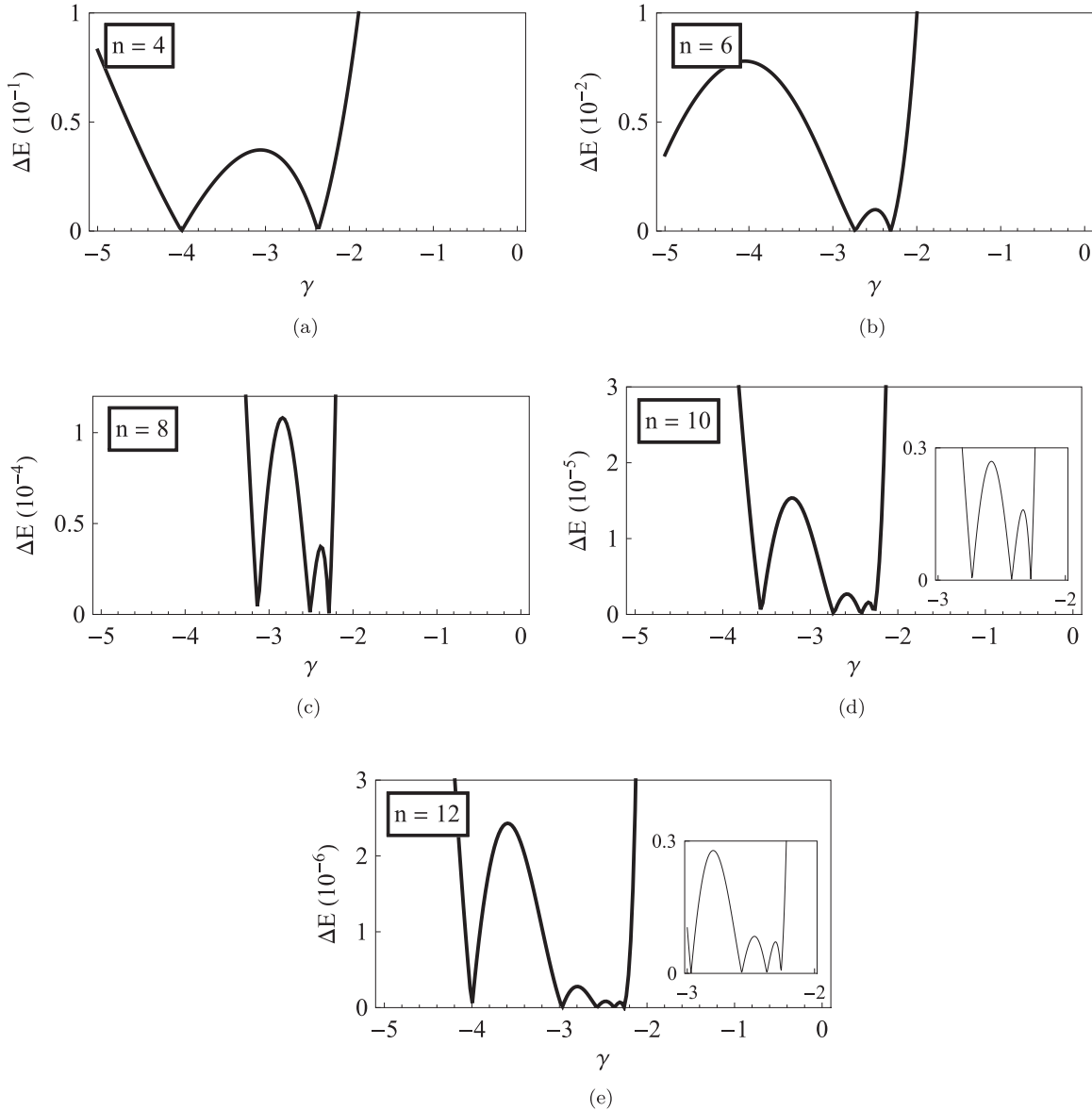
FIG. 10. Dimensionless energy gap as a function of the dimensionless coupling γ for (a) $n = 4$, (b) $n = 6$, (c) $n = 8$, (d) $n = 10$, and (e) $n = 12$. We set the parameters $\lambda = 2$ and $\beta = 0$ in all cases. The presence of nonzero regions for ΔE indicates that there are level crossings between the ground state and the first excited state at some particular values of γ.

some roots approach 0, others diverge due to the invariance $v_j \rightarrow v_j^{-1}$. It should be noted that this change from positive to negative roots has no relation to the quantum phase transition in this model.

In Figs. 8 and 9 we plot solutions of the BAE for certain values of the total number of particles n. These numerical solutions agree with the exact diagonalization of the Hamiltonian. Starting with Fig. 8, we plot the solutions to the BAE, (15), with $n = 4$. The roots generally evolve smoothly as the value of the parameter $\gamma = n\Omega/J$ varies, although for some particular values the trajectories exhibit jumps. This same characteristic behavior of the ground-state roots is observed for other values of n (see Fig. 9).

Examination of the energy levels of the system for small numbers of particles shows that there are crossings of levels between the ground state and the first excited state, detected

due to the presence of nonzero regions in the energy gap. Note that the number of nonzero regions in the energy gap increases along with the number of particles, while its amplitude decreases (in fact, Fig. 10 shows that the amplitude of the nonzero regions of the energy gap becomes $10\times$ lower every time we add two particles to the system). We also note that, as the number of particles increases, the solutions of the BAE still predict the crossing of energy levels, despite the small value of ΔE.

IV. SUMMARY

In this work we have introduced an eTMBH model with a nonlinear tunneling interaction term. We found that the model exhibits quantum phase transitions between three phases: a Josephson phase, a self-trapping phase, and a phase-locking

phase. This result was obtained through a classical analysis, allowing for the identification of the parameter space of phase transitions as depicted in Fig. 6. For the case $\lambda > 0$, we compared the predictions arising from the classical analysis with the energy gap. It was found that the boundary between the Josephson and the phase-locking regimes coincides with the closing of the gap.

We have then presented the exact solution for this model using the Bethe ansatz method. Guided by the location of quantum phase transition boundaries predicted by the classical analysis, we analyzed solutions of the BAE and the energy gap for small numbers of particles. Crossing of levels between the ground state and the first excited state were detected. As we increase the number of particles, the crossings between these two states become more frequent, and between crossings the range of the dimensionless gap ΔE occurs on a smaller scale. The onset of these crossings in the few particle system may be viewed as the analog of the quantum phase transition between the phase-locking and the Josephson phases identified from the classical analysis, which assumes a large particle number. Significantly, the level crossings occur even in the case of only four particles. It is important to emphasize that the level

crossings are a feature of the atom-pair tunneling interaction, and they are not present when $\Omega = 0$ or, equivalently, $\gamma = 0$. This is consistent with the fact that line $\gamma = 0$ does not intersect the phase-locking phase in Fig. 6.

The unusual features uncovered in this study call for a deeper analysis of the exact solution of the model. In future work it is planned to extend the methods adopted in [28] and [29] to the TMBH model to meet this need. It would also be of tremendous interest to realize a double-well trap with an enhanced atom-pair tunneling coupling, via the lattice shaking techniques advocated in [16]. Significantly, lattice shaking methods have recently been used to successfully drive a cold-atom system through a quantum phase transition [30].

[1] M. Albiez, R. Gati, J. Folling, S. Hunsmann, M. Cristiani, and M. K. Oberthaler, Phys. Rev. Lett. **95**, 010402 (2005).

[2] A. J. Leggett, Rev. Mod. Phys. **73**, 307 (2001).

[3] G. J. Milburn, J. Corney, E. M. Wright, and D. F. Walls, Phys. Rev. A **55**, 4318 (1997).

[4] A. P. Hines, R. H. McKenzie, and G. J. Milburn, Phys. Rev. A **67**, 013609 (2003).

[5] J. R. Anglin, P. Drummond, and A. Smerzi, Phys. Rev. A **64**, 063605 (2001).

[6] H.-Q. Zhou, J. Links, R. H. McKenzie, and X.-W. Guan, J. Phys. A: Math. Gen. **36**, L113 (2003).

[7] A. P. Tonel, J. Links, and A. Foerster, J. Phys. A **38**, 1235 (2005).

[8] F. Pan and J. P. Draayer, Phys. Lett. A **339**, 403 (2005).

[9] A. Trenkwalder, G. Spagnolli, G. Semeghini, S. Coop, M. Landini, P. Castilho, L. Pezzé, G. Modugno, M. Inguscio, A. Smerzi, and M. Fattori, Nat. Phys. **12**, 826 (2016).

[10] S. Fölling, S. Trotzky, P. Cheinet, M. Feld, R. Saers, A. Widera, T. Muller, and I. Bloch, Nature **448**, 1029 (2007).

[11] S. Zöllner, H.-D. Meyer, and P. Schmelcher, Phys. Rev. Lett. **100**, 040401 (2008).

[12] D. Ananikian and T. Bergeman, Phys. Rev. A **73**, 013604 (2006).

[13] R. Gati and M. K. Oberthaler, J. Phys. B **40**, R61 (2007).

[14] J.-Q. Liang, J.-L. Liu, W.-D. Li, and Z.-J. Li, Phys. Rev. A **79**, 033617 (2009).

[15] J.-L. Liu and J.-Q. Liang, Mod. Phys. Lett. B **25**,2137 (2011); J. Phys. B **44**, 025101 (2011).

[16] Q. Zhu, Q. Zhang, and B. Wu, J. Phys. B **48**, 045301 (2015).

[17] S. Dutta, A. Barman, A. Siddharth, A. Khan, and S. Basu, Eur. Phys. J. B **88**, 139 (2015).

[18] L. Wen, Q. Zhu, T. Xu, X. Jing, and C.-S. Liu, J. Phys. B **49**, 015303 (2016).

[19] B. Wu and J. Liu, Phys. Rev. Lett. **96**, 020405 (2006).

[20] S. Raghavan, A. Smerzi, S. Fantoni, and S. R. Shenoy, Phys. Rev. A **59**, 620 (1999).

[21] J. Links, A. Foerster, A. P. Tonel, and G. Santos, Ann. Henri Poincare **7**, 1591 (2006).

[22] A. P. Hines, R. H. McKenzie, and G. J. Milburn, Phys. Rev. A **71**, 042303 (2005).

[23] S. Schneider and G. J. Milburn, Phys. Rev. A **65**, 042107 (2002).

[24] J. Liu, B. Wu, and Q. Niu, Phys. Rev. Lett. **90**, 170404 (2003).

[25] S. Sachdev, *Quantum Phase Transitions*, 2nd ed. (Cambridge University, Cambridge, UK, 2011).

[26] V. Z. Enol'skii, V. B. Kuznetsov, and M. Salerno, Phys. D **68**, 138 (1993).

[27] J. Links and S.-Y. Zhao, J. Stat. Mech. (2009) P03013.

[28] D. Rubeni, E. Mattei, A. Foerster, and I. Roditi, Nucl. Phys. B **856**, 698 (2011).

[29] J. Links and I. Marquette, J. Phys. A **48**, 045204 (2015).

[30] L. W. Clark, L. Feng, and C. Chin, Science **354**, 606 (2016).